

PAPER

Hydrogen bubble nucleation by self-clustering: density functional theory and statistical model studies using tungsten as a model system

To cite this article: Jie Hou *et al* 2018 *Nucl. Fusion* **58** 096021

View the [article online](#) for updates and enhancements.

Related content

- [First-principles calculations of transition metal solute interactions with hydrogen in tungsten](#)
- [Super-saturated hydrogen effects on radiation damages in tungsten under the high-flux divertor plasma irradiation](#)
- [A review of modelling and simulation of hydrogen behaviour in tungsten at different scales](#)

Recent citations

- [Enhanced H-H binding and consequent H-aggregation around dislocation in -Fe lattice](#)
Yanguang Cui *et al*
- [\(001\) edge dislocation nucleation mechanism of surface blistering in tungsten exposed to deuterium plasma](#)
Wanguo Guo *et al*

**IOP | ebooks™**

Bringing together innovative digital publishing with leading authors from the global scientific community.

Start exploring the collection—download the first chapter of every title for free.

Hydrogen bubble nucleation by self-clustering: density functional theory and statistical model studies using tungsten as a model system

Jie Hou^{1,2,3}, Xiang-Shan Kong¹, Jingjing Sun^{1,2}, Yu-Wei You¹, Xuebang Wu¹, C. S. Liu¹  and Jun Song³

¹ Key Laboratory of Materials Physics, Institute of Solid State Physics, Chinese Academy of Sciences, PO Box 1129, Hefei 230031, China

² University of Science and Technology of China, Hefei 230026, China

³ Department of Mining and Materials Engineering, McGill University, Montréal, Québec H3A 0C5, Canada

E-mail: xskong@issp.ac.cn (X.S. Kong), csliu@issp.ac.cn (C.S. Liu) and jun.song2@mcgill.ca (J. Song)

Received 26 February 2018, revised 24 April 2018

Accepted for publication 20 June 2018


Published 10 July 2018



Abstract

Low-energy, high-flux hydrogen irradiation is known to induce bubble formation in tungsten, but its atomistic mechanisms remain little understood. Using first-principles calculations and statistical models, we studied the self-clustering behaviour of hydrogen in tungsten. Unlike previous speculations that the hydrogen self-clusters are energetically unstable owing to the general repulsion between two hydrogen atoms, we found that 2D platelet-like hydrogen self-clusters could form at high hydrogen concentrations. The attractive binding energy of the hydrogen self-cluster becomes larger as the cluster size increases and plateaus at 0.38 eV/H around size of 40. We found that hydrogen atoms would form 2D platelet-like structures along $\{100\}$ planes. These hydrogen self-clustering behaviours can be quantitatively understood by the competition between long-ranged elastic attraction and local electronic repulsion among hydrogens. Further analysis showed hydrogen self-clusters to be kinetically feasible and thermodynamically stable above a critical hydrogen concentration. Based on this critical hydrogen concentration, we predicted the hydrogen irradiation condition required for the formation of hydrogen self-clusters. Our predictions showed excellent agreement with the experimental results of hydrogen bubble formation in tungsten exposed to low-energy hydrogen irradiation. Finally, we proposed a possible mechanism for the hydrogen bubble nucleation via hydrogen self-clustering. This work provides mechanistic insights and quantitative models towards understanding of plasma-induced hydrogen bubble formation in plasma-facing tungsten.

Keywords: hydrogen self-clustering, hydrogen bubble, tungsten, first-principles calculations

 Supplementary material for this article is available [online](#)

(Some figures may appear in colour only in the online journal)

1. Introduction

Hydrogen (H) bubble formation, and the consequent hydrogen embrittlement that often results, poses a great threat to the structural integrity and mechanical properties of

metals; this in turn has prompted extensive studies over the years [1–4]. Several mechanisms, including ‘loop punching’ and ‘vacancy clustering’, have been proposed to explain the hydrogen bubble growth [4]. While these mechanisms are quite distinct in nature, they all require a nucleation process

for the hydrogen bubble growth to occur. To date, it has generally been believed that hydrogen bubble nucleation by self-clustering (as with helium in metals [5, 6]) is impossible given the strong H–H repulsion or very weak attraction in metals [7–14]. Consequently, as suggested by many previous studies [4, 7, 8, 10, 11], hydrogen bubble nucleation would require the presence of lattice defects. The hydrogen bubble nucleation can either be heterogeneous, relating to grain boundaries [15–18], dislocations [18–21], and impurities [7, 22]; or homogeneous, arising from the aggregation of vacancies or vacancy-hydrogen complexes [23, 24]. However, hydrogen bubble formation in metals with extremely low concentration of lattice defects has been clearly observed in many experiments [25–46]. In particular, one of the most commonly studied phenomena over the past decade has been hydrogen bubble formation in well-annealed tungsten (nearly free of dislocations and vacancies) after high-flux low-energy hydrogen irradiation [28–46].

Since tungsten has been considered the primary candidate for the plasma-facing material (PFM) of fusion reactors, hydrogen bubble formation in tungsten has received great attention. Hydrogen bubble formation in tungsten not only leads to instability of the plasma, but also increases tritium inventory in the PFM [33]. Despite extensive research studies, it is still an open question as to how hydrogen bubbles manage to nucleate during low-energy and high-flux hydrogen plasma irradiations. On one hand, the low energy of hydrogen plasma used in the experiments is far lower than the threshold energy required to induce any displacement damage in tungsten for the formation of new self-interstitial atoms or vacancies. On the other hand, in most of those previous experiments [20, 29, 31–43], annealed pure tungsten samples with coarse-grained or single crystal structures were used, which minimizes the influence of the intrinsic defects, such as dislocations, vacancies, and grain boundaries, produced during the sample preparation. Furthermore, the formation energies of lattice defects in tungsten are very high. For instance, even for the simple point defect, i.e. a single vacancy, the formation energy is about 3.2 eV [22], which corresponds to an extremely low vacancy concentration (about 10^{-54} , in atomic ratio, similarly hereinafter) at room temperature and even at the annealing temperature (e.g. about 10^{-13} at 1270 K). Therefore, population of lattice defects in well-annealed, undamaged tungsten is expected to be rather limited, being insufficient to provide enough nucleation sites for hydrogen bubble formation.

The aforementioned puzzle regarding hydrogen bubble nucleation has stimulated many dedicated studies. Poon *et al* argued that plasma impurities such as carbon and oxygen have energy transfer efficiencies higher than that of hydrogen isotopes, and therefore can more easily create vacancies to supply nucleation sites when tungsten is exposed to a 500 eV deuterium plasma [28]. However, this mechanism cannot be applied to other experiments where hydrogen bubbles were observed after being exposed to deuterium plasma with energy of tens of eV [33–42, 44–46]. To explain these experiments [33–42, 44–46], Shu *et al* employed Fukai's superabundant vacancies (SAV) theory [33, 34], attributing the high vacancy concentration to the significant reduction of the vacancy formation

energy by vacancy-H binding [47–49]. Nonetheless, a recent theoretical study by Kong *et al* [22] showed that vacancy-H complexes in tungsten can only reduce the vacancy formation energy to ~ 2.45 eV, which is insufficient to produce a high vacancy concentration ($\sim 10^{-39}$ at room temperature). Furthermore, to overcome kinetic barriers, the SAV formation often requires high temperatures which are not available in many hydrogen bubble formation experiments around room temperature [28–42]. Kong *et al* showed that oxygen impurities can significantly decrease the vacancy formation energy in tungsten, and suggested that the vacancy concentration may be enhanced by the formation of vacancy-oxygen-hydrogen complexes [22]. However, hydrogen nano-bubbles were only observed in the subsurface region in recent experiments, indicating no obvious relationship of hydrogen bubble formation with the impurities [46]. The nucleation mechanisms proposed by the preceding studies are related to the vacancy formation. Though they have their individual merits and may operate under certain conditions, they are not general and fundamental enough to provide quantitative explanations of hydrogen bubble nucleation in tungsten exposed to low-energy and high-flux hydrogen plasma irradiations. Moreover, hydrogen bubble formation was frequently observed at around room temperature [29–42], at which the vacancies or vacancy-hydrogen complexes, even if they exist with high concentrations, would be immobile and thus not able to gather together to form bubbles.

Apart from the vacancies, it has also been suggested that dislocations can be responsible for hydrogen bubble formation [19–21]. Terentyev *et al* [19] proposed that hydrogen clusters can be formed around dislocations, which eventually result in the punching of a jog, providing room for bubble nucleation. In recent experiments [20, 43], the presence of pre-existing dislocation showed significant influences on hydrogen bubble formation. However, the plasma-induced hydrogen bubble formation was also widely observed in fully recrystallized tungsten with very low dislocation densities [20, 33, 34, 43]. In addition, some recent experiments showed that hydrogen plasma loading can induce plastic deformation along with large density of dislocations in tungsten [50]. How these abundant dislocations can be created without external strain remains to be elusive.

Recently, by analyzing the spatial distribution of low-energy hydrogen-induced defects, Ni *et al* [42] and Jia *et al* [46] found that the hydrogen bubble distribution is homogeneous inside the grain, and is independent of the pre-existing vacancies, impurities, dislocations, or grain boundaries. This suggests the existence of a possible hydrogen bubble nucleation mechanism independent of pre-existing lattice defects. Alimov *et al* have proposed a void formation mechanism to explain the sudden rise in deuterium trapping sites and the concurrent deuterium accumulation in tungsten exposed to 200 eV deuterium ions [29]. They suggested that excessive interstitial deuterium atoms in the implantation zone severely stress the tungsten lattice and subsequently cause formation of voids or vacancy clusters to alleviate these tensions. Unfortunately, no atomic detail has been given to support this suggestion. In addition, it is worth noting that some early studies suggested the

Table 1. Supercells and k -point grids used for simulating hydrogen self-clusters of different sizes, together with the corresponding partial volume of hydrogen.

	Supercell	k -point	Partial volume (nm ³)
H _{≤16} , H _∞	6 × 6 × 4	2 × 2 × 3	2.98 × 10 ⁻³
H _{24–36}	8 × 8 × 4	1 × 1 × 2	2.86 × 10 ⁻³

aggregation of hydrogen in a platelet shape in metals, which can alleviate the strain induced by the excessive interstitial hydrogen atoms [51, 52]. In this work, we focus on the self-clustering behaviour of hydrogen, i.e. hydrogen clustering in a defect-free tungsten lattice. First-principles calculations are carried out to explore possible hydrogen self-cluster structures and identify the most favorable ones. We find that hydrogen self-clusters prefer to form planar structures within {100} planes. We show that self-clustering behaviour can be well described by the competition between elastic attraction and electronic repulsion. Based on the planar hydrogen self-clustering, we propose a bubble-formation mechanism in defect-free tungsten. Further statistical evaluations show that the self-clustering is thermodynamically favorable and kinetically feasible at high hydrogen concentrations. Our results provide quantitative explanation for previous experiments where bubbles were induced by low-energy hydrogen plasma.

2. Computation method

First-principles calculations on the basis of density functional theory (DFT) as implemented in the Vienna *ab initio* simulation package [53, 54] with Blochl's projector augmented wave (PAW) potential method [55] were performed. All 5d and 6s electrons of tungsten and the 1s electron of hydrogen were treated as valence electrons in the PAW potential. The exchange-correlation energy functional was described with the generalized gradient approximation as parameterized by Perdew–Wang (PW91) [56, 57]. Two sets of supercells and k -point grids were used for different sizes of hydrogen self-clusters, as shown in table 1. Relaxations of atomic configuration and optimizations of the shape and size of the super-cell were performed for all calculations unless stated otherwise. A plane wave cutoff of 500 eV was used in these calculations. Benchmark calculations with increased super-cell size, cutoff energy, and k -point density have been carried out, and negligible influence on our results was found. The convergence criteria of system energy and atomic force were set as 1 μ eV and 0.1 eV nm⁻¹ respectively in our calculations.

The binding energy of an isolated interstitial hydrogen atom with a stable H_{*n*-1} self-cluster is calculated as:

$$E_b^{H_n} = E_{\text{tot}}^{H_{n-1}} + E_{\text{tot}}^{H_1} - (E_{\text{tot}}^{H_n} + E_{\text{tot}}^{\text{bulk}}), \quad (1)$$

where $E_{\text{tot}}^{H_n}$ and $E_{\text{tot}}^{\text{bulk}}$ are energies of super-cells with and without a H_{*n*} self-cluster. A negative value of the binding energy indicates repulsion between two defects, while the positive value means attraction. The solution energy of an isolated interstitial hydrogen atom in tungsten is calculated as:

$$E_s = E_{\text{tot}}^{H_1} - E_{\text{tot}}^{\text{bulk}} - \frac{1}{2}E^{H_2}, \quad (2)$$

where E^{H_2} is the energy of a H₂ molecule in vacuum.

In addition, the zero-point energy (ZPE) correction, which can play an important role for light elements, was also included in this work to ensure accurate description of energies of hydrogen and hydrogen self-clusters. The binding energy and solution energy with ZPE corrections are given by:

$$E_b^{H_n}(\text{ZPE}) = E_b^{H_n} + E_{\text{ZPE}}^{H_{n-1}} + E_{\text{ZPE}}^{H_1} - E_{\text{ZPE}}^{H_n}, \quad (3)$$

$$E_s(\text{ZPE}) = E_s + E_{\text{ZPE}}^{H_1} - \frac{1}{2}E_{\text{ZPE}}^{H_2}, \quad (4)$$

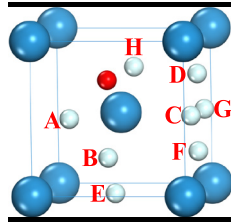
where $E_{\text{ZPE}}^{H_n}$ is total zero-point energy of the H_{*n*} self-cluster, and $E_{\text{ZPE}}^{H_2}$ is the total zero-point energy of a H₂ molecule in vacuum. It is worthy to note that the binding and solution energies may also be affected by the phonon excitation [58] and ZPE of the tungsten atom. However, such effects are negligible and thus not considered here for computational efficiency⁴.

3. Results and discussion

3.1. Configurations and binding energetics of stable H_{*n*} self-clusters

It is well known that, in tungsten, an interstitial hydrogen atom prefers to occupy the tetrahedral interstitial site (TIS) rather than the octahedral interstitial site (OIS), and the interstitial H–H interaction is generally repulsive [7–11]. These results have also been confirmed by our current calculations, where the TIS is found to be 0.38 eV more stable than the OIS for a hydrogen atom. Our preliminary calculations also show that all TIS–OIS hydrogen pairs, OIS–OIS hydrogen pairs, OIS hydrogen self-clusters are energetically unfavorable or unstable compared with the pure TIS ones. Therefore, we only consider TIS hydrogen atoms in this study. Figure 1 summarizes the binding energies between two hydrogen atoms located at 1 nn to 8 nn neighboring TIS sites. As shown in figure 1, the binding energy of the H–H pairs is strongly negative (~ -0.46 eV) at a distance of ~ 0.154 nm, then increases rapidly with the increase of the H–H separation distance and becomes a small positive value (~ 0.01 eV) at a distance of ~ 0.222 nm. With further increasing distance, the binding energy decreases into a small negative value again before it eventually diminishes to zero. These results suggest that the two interstitial hydrogen atoms in tungsten are mostly repulsive. Our results are also in good agreement with results previously reported [7–11]. However, it is worth noting that two particular cases of H–H pairing yields positive binding energies, one being two hydrogen atoms located at the 4 nn neighboring TIS sites to form a H–H pair along the $\langle 110 \rangle$ direction, and the other being two located at the 5 nn neighboring TIS sites to form a H–H pair along the $\langle 310 \rangle$ direction. Despite the attractive interaction being weak, this hints at the

⁴ See supplemental material (stacks.iop.org/NF/58/096021/mmedia).



	The binding energy of H-H (in unit of eV)				The distance between H-H (in unit of nm)		
	Present		Ref.[9]	Ref.[10]	Present	Ref.[9]	Ref.[10]
	ZPE	No ZPE					
A (1nn)	-0.37	-0.46	-0.47	-0.45	0.1544	0.1524	0.1530
B (2nn)	-0.10	-0.12	-0.11	-0.09	0.1802	0.1777	0.1790
C (3nn)	-0.01	-0.03	-0.03	-0.03	0.1986	0.1968	0.1980
D (4nn)	0.02	0.01	0.01	0.02	0.2228	0.2222	0.2220
E (5nn)	0.01	0.00	0.00	0.01	0.2494	0.2476	0.2480
F (6nn)	0.00	-0.01		-0.01	0.2762		0.2750
G (7nn)	-0.03	-0.03	-0.03	-0.04	0.3006	0.2984	0.2980
H (8nn)	-0.05	-0.05	-0.05	-0.04	0.3223	0.3174	0.3210

Figure 1. The binding energies between two hydrogen atoms located at 1nn to 8nn neighboring TIS sites, calculated using equations (1) and (3). The insert figure shows spatial relationship between two hydrogen atoms. The large mineral blue balls are tungsten atoms. The small red ball marks out position of the reference hydrogen atom while the small white balls, denoted by letters A ~ H, indicate positions of the second hydrogen atom at 1nn–8nn neighboring TIS sites.

possibility of forming hydrogen self-clusters along particular directions or within particular planes. Moreover, some previous studies on inert-gas self-clusters in tungsten have suggested that attraction between interstitial atoms may become stronger as the local aggregation grows [5, 6], eventually leading to large self-clusters. In analogy to those studies, it is important to investigate if a similar scenario would occur for H–H interaction to finally promote the formation of sizable hydrogen self-clusters, as elaborated in the following.

In order to check the possibility of interstitial hydrogen self-cluster (H_n) formation, we first constructed a series of plausible geometries. One hydrogen atom was placed in different TISs neighboring the stable and metastable H_{n-1} ($n > 2$) complexes in turn, and then the total energies of these systems were minimized to identify the most stable configuration of the resultant H_n self-clusters. However, because of the overwhelming number of possible combinations of the H_{n-1} self-cluster and additional hydrogen, it is impossible to screen all possible configurations. To overcome this challenge, we utilized two criteria to select possible positions for an additional hydrogen atom introduced to the vicinity of the H_{n-1} cluster: (1) the additional hydrogen atom, when introduced, forms the $\langle 110 \rangle$ or $\langle 310 \rangle$ H–H pairs with those original hydrogen atoms within H_{n-1} , as many as possible; (2) the distance between the newly introduced hydrogen and an original hydrogen within H_{n-1} is greater than 0.2 nm (≥ 3 nn) [59].

Using the strategy just described, we systematically investigated hydrogen self-clusters in three different shapes: spherical, linear, and planar. Figure 2 illustrates the energetically preferable configurations for each of these self-cluster shapes. The corresponding binding energies, as functions of the cluster size n , are shown in figure 3. It is clearly shown that spherical configurations are not stable, with their binding energies being generally negative. The binding energies for linear hydrogen self-clusters have small positive values, suggesting that the self-clustering is energetically favorable. Specifically for the

linear hydrogen cluster, hydrogen atoms prefer to arrange along the $\langle 110 \rangle$ directions. This arrangement ensures that all the closest H–H pairs are in the most stable binding state. From figure 3, we also observe that the planar structure appears to be the most stable structure of hydrogen self-clusters (except for $n = 3$). Particularly worth noting is that the binding energy of planar self-clusters increases overall with the cluster size. This increasing tendency indicates that the ability of a H_n platelet to capture isolated interstitial hydrogen atoms grows with its self-cluster size n , which may trigger a cascading procedure of hydrogen self-clustering in high hydrogen concentration environments. In the planar self-cluster, the hydrogen atoms prefer to aggregate within the $\{100\}$ planes, which ensures that all the closest H–H pairs are in the most stable $\langle 110 \rangle$ binding state, similar to the case of the linear hydrogen self-clusters. One additional thing worth noting is that, despite the $\langle 310 \rangle$ H–H pairs also being energetically favorable, this pairing does not seem to show a particular influence on the linear or planar aggregation of hydrogen atoms, likely owing to symmetry reasons.

3.2. Physical origin underlying H–H interaction

The H–H interaction in metal mainly comprises two effects, i.e. the elastic interaction and the electronic interaction. The elastic interaction arises from the lattice dilatation induced by interstitial hydrogen, i.e. the introduction of an interstitial hydrogen into a perfect metal lattice distends its neighbouring interstitial sites, which provides more space for subsequent insertion of interstitial hydrogen, and consequently resulting in an attractive interaction among the interstitial hydrogen atoms. In order to assess the elastic interaction quantitatively, we first investigated the behaviour of an interstitial hydrogen atom under isotropic strains. Figure 4 shows the hydrogen solution energy as a function of the strain. Interestingly, we found that the solution energy varies linearly with the volumetric strain, and can be well described by [15]:

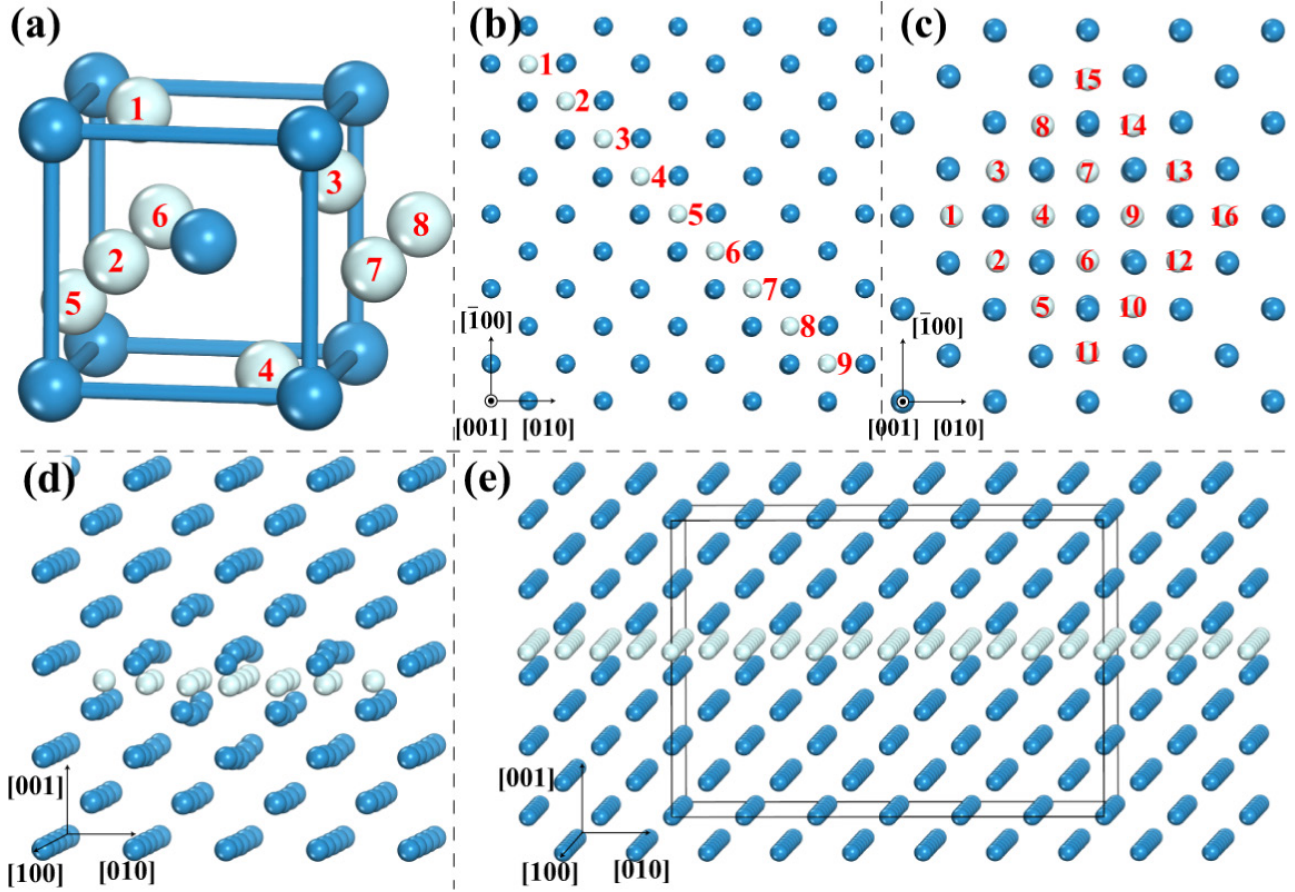


Figure 2. Configurations of hydrogen self-clusters. Tungsten and hydrogen atoms are in blue (balls/lines) and white, respectively. The red numbers represent hydrogen occupation sequence. (a) and (b) Illustrate the most stable spherical hydrogen and linear hydrogen self-clusters, respectively, along the $[110]$ direction. (c) and (d) show the top and side views, respectively, of the most stable planar H_n self-cluster in a (001) plane. (e) Shows the planar $H_{n \rightarrow \infty}$ self-cluster in a periodic supercell.

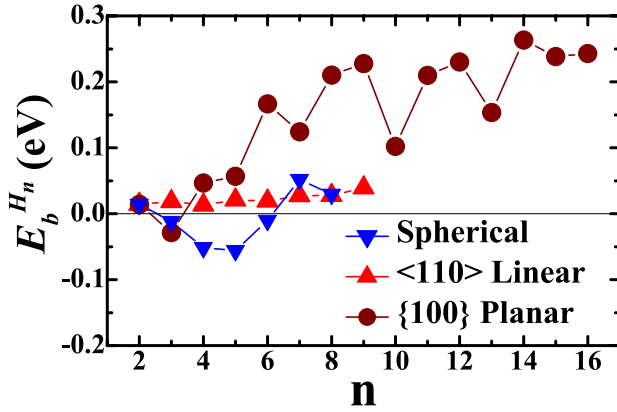


Figure 3. Binding energies of hydrogen self-clusters (i.e. those previously shown in figure 2) as the cluster size n varies.

$$E_s = E_s^0 - B\Omega_H \frac{\Delta V_{\text{tet}}}{V_{\text{tet}}^0}. \quad (5)$$

Here, E_s^0 is hydrogen solution in tungsten when no strain is applied; B is the bulk modulus, being 310 GPa for tungsten; Ω_H is the partial volume of a hydrogen atom in tungsten, being $\sim 3 \times 10^{-3} \text{ nm}^3$ [15, 60]; V_{tet}^0 is the tetrahedron volume in the perfect tungsten lattice; and ΔV_{tet} is the tetrahedron volume change induced by the isotropic strain. This

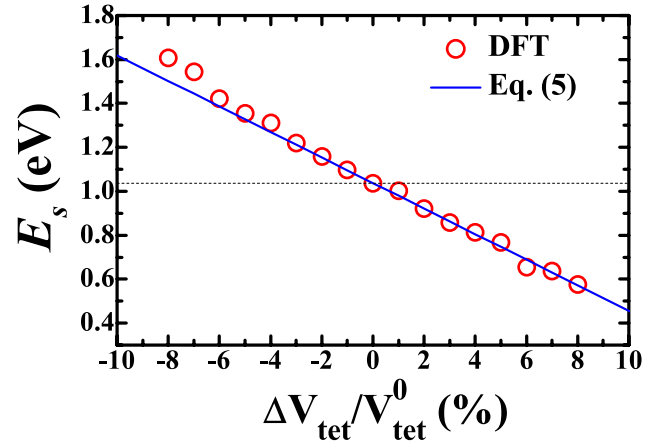


Figure 4. Hydrogen solution energy as a function of tetrahedron volume change under isotropic strain.

equation gives us a simple analytical means to evaluate the elastic interaction between interstitial hydrogen atoms. The excellent agreement between model prediction and DFT calculated data shown in figure 4 also suggests that the effect of deformation on H solution energy is dominantly isotropic. According to our definition in equations (1) and (2), we could estimate the elastic contribution of $E_b^{H_n}$ using an elastic binding energy:

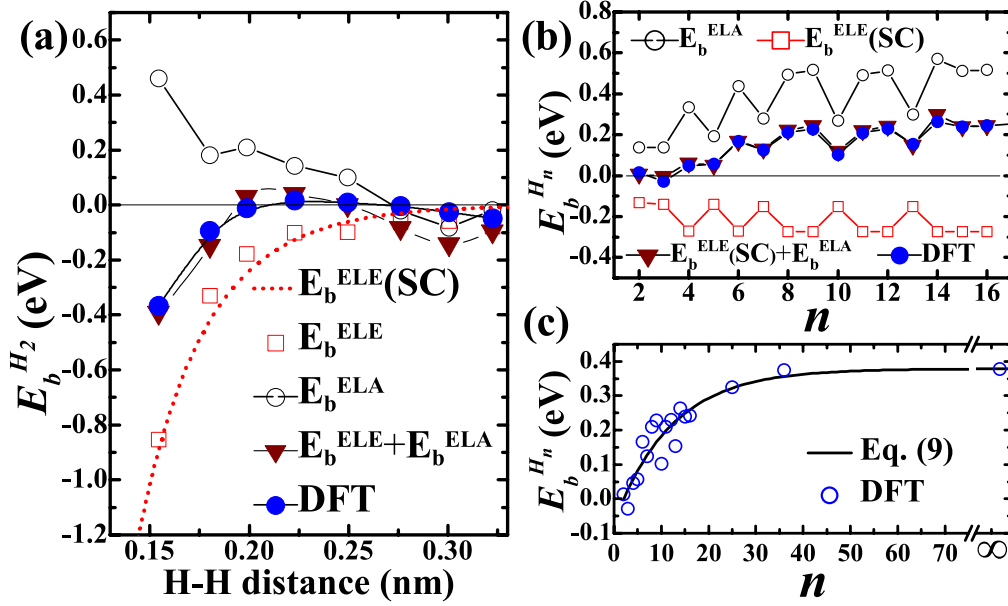


Figure 5. (a) Elastic (ELA) and electronic (ELE) contributions of H-H binding energies at different H-H separation distance. SC represents electronic binding energy fitted using equation (7). (b) Binding energies of the most stable planar $H_{2\sim 16}$ self-clusters, along with a similar analysis of the corresponding elastic and electronic contributions. (c) The evolution of binding energy of a H_n cluster as the cluster size n varies, and the fitted curve (solid black line) using equation (9). For $n = 25$ and 36 , DFT results are calculated using a $8 \times 8 \times 4$ supercell with a $1 \times 1 \times 2$ k -point grid. For $n \rightarrow \infty$, the DFT result is calculated according to equation (8).

$$E_b^{ELA} = B\Omega_H \frac{\Delta V_{tet}}{V_{tet}^0}, \quad (6)$$

where ΔV_{tet} is the volume change of the neighboring tetrahedron induced by a H_{n-1} self-cluster. Note the elastic binding is not a direct interaction between H interstitials, but an indirect one mediated by neighboring W atoms.

The electronic interaction comes from the change of the hydrogen states in the electronic structure. For two hydrogen ions in close vicinity, the bonding and antibonding states between them will shift asymmetrically and raise the total energy [9, 13]. Consequently, this leads to a repulsive interaction between H-H pairs. The electronic interaction can also be characterized by an electronic binding energy, E_b^{ELE} . Unfortunately, to the best of our knowledge, there is no analytical formula to evaluate the electronic binding energy. Here, the E_b^{ELE} was estimated by the binding energies of hydrogen atoms in a frozen lattice where both supercell and atom positions were fixed.

The binding energies, and corresponding elastic and electronic contributions associated with hydrogen self-clusters are shown in figure 5. Let us start by examining the situation of H-H pairs, i.e. H_2 self-clusters, in tungsten (see figure 5(a)). We can see that the sum of E_b^{ELA} and E_b^{ELE} is in excellent agreement with the DFT-calculated binding energy. This good agreement confirms that the H-H interaction in tungsten is indeed contributed by the elastic and electronic interactions. In particular, the elastic interaction is generally positive while the electronic interaction is negative, which suggests that they respectively correspond to attraction and repulsion between two hydrogen atoms. Both elastic and electronic interactions decrease in magnitude as the H-H distance increases, with the

electronic interaction being much stronger at short distance but decaying more rapidly with the distance. The domination of electronic repulsion at short distances explains the fact that two interstitial hydrogen atoms are mutually exclusive at short distances (< 0.2 nm). As the H-H distance increases from 0.2 to 0.25 nm, the elastic attraction starts to surpass the electronic repulsion. Thus, the H-H pairs are in binding states at this range. With further increasing distance, both interactions approach zero, and the elastic interaction also changes to being negative, rendering the overall H-H interaction as weak repulsion. Consequently, it can be concluded that the competition and interplay of the elastic and electronic contributions prescribe the behaviours of H-H pairs, and subsequently are expected to control the behaviours of hydrogen self-clusters. In this regard, in the following we perform a similar analysis for hydrogen self-clusters to elucidate the physical origin of hydrogen self-clustering.

One particular interesting observation to note from figure 4(a) is that the electronic interaction can be well fitted with a screened Coulomb (SC) potential [61]:

$$E_b^{ELE(SC)} = -\frac{q^2}{4\pi\epsilon_0 r} \exp(-k_s r), \quad (7)$$

where q corresponds to the effective charge on each hydrogen, ϵ_0 is the vacuum permittivity, r is the H-H separation distance, and $k_s = \sqrt{\frac{4}{a_0} \left(\frac{3n_0}{\pi}\right)^{\frac{1}{3}}}$ is the screening parameter with n_0 being the electron density and a_0 being the Bohr radius [61]. Here, all 5d and 6s electrons in tungsten are treated as free electrons, which yield $k_s = 231.6 \text{ nm}^{-1}$. Fitting the DFT-computed E_b^{ELE} data to equation (7), we obtained $q = 1.85 e$, which is very close to the hydrogen charge estimated by the Bader's charge analysis [62, 63], $q = 1.86 e$. This good agreement suggests

that the electronic interaction between hydrogen atoms can be well estimated with the screened Coulomb interaction. Equation (7) provides a simple analytical means to evaluate E_b^{ELE} , and is used subsequently in the analysis of binding energies of hydrogen self-clusters.

Figure 5(b) presents the binding energies of an additional interstitial hydrogen atom with the stable H_{n-1} cluster. The corresponding elastic and electronic interactions respectively predicted from equations (6) and (7) are also shown for comparison. The electronic interaction for a H_n self-cluster is calculated by summing up all the pairwise E_b^{ELE} terms (from equation (7)) between the n th hydrogen atom and each hydrogen atom in the H_{n-1} cluster. Similar to what was previously observed in figure 5(a), the sum of elastic and electronic contributions well agrees with the DFT-calculated binding energy, again showing that the elastic and electronic interactions prescribe the H–H interaction in tungsten. Figure 5(b) also demonstrates that equations (6) and (7) provide a description model to quantitatively analyze the interstitial hydrogen self-clustering in tungsten lattice. This modeling framework is quite general and can be applied to study the self-clustering behaviours of other impurities in metals. For instance, benchmark calculations have been performed to show that it's also possible to use this model to explain the self-clustering of helium in tungsten⁵.

We note from figure 5(b) that the electronic interaction only alternates between two distinct energy states of -0.14 and -0.27 eV in the range of self-cluster sizes investigated. This is because the electronic interaction is very much localized and becomes negligible for H–H distance beyond 0.3 nm. Consequently the newly introduced hydrogen atom, i.e. the n th hydrogen, only interacts with its nearest-neighboring hydrogen atoms in the H_{n-1} self-cluster. For instance, for the case shown in figure 2(c), in terms of electronic interaction, the 16th hydrogen only interacts with the 12th and the 13th hydrogens in the H_{15} cluster, as the distance from any other hydrogen to the 16th hydrogen is >0.32 nm. As the self-cluster size n varies, there exist only two scenarios for the electronic interaction: that the n th hydrogen interacts with one (for $n = 2, 3, 5, 7, 10, 13, \dots$) or two (for $n = 4, 6, 8, 9, 11, 12, 14, 15, \dots$) nearest-neighboring hydrogens in the H_{n-1} self-cluster. These two scenarios correspond to the two distinct energy states of -0.14 eV and -0.27 eV respectively, leading to the electronic interaction alternation as the H_n self-cluster grows.

On the other hand, the elastic interaction overall exhibits an increasing trend as the self-cluster size n increases. The trend indicates that the elastic attraction would gradually overcome the local electronic repulsion as the self-cluster grows. As we previously discussed, planar structure is the most favorable structure of hydrogen self-clusters, and the elastic interaction comes from the expansion of interstitial sites near a hydrogen cluster. Clearly, the insertion of a hydrogen platelet into a tungsten lattice will cause sizable lattice expansion, particularly around the platelet edge. The appreciable expansion at the edges provides more space for

interstitial hydrogen atoms, making it energetically more favorable for hydrogen occupancy and thus resulting in the planar growth of the hydrogen cluster. As the self-cluster grows, the degree of lattice swelling is expected to increase. However, presumably the lattice swelling would eventually plateau, and it is anticipated that the binding energy of hydrogen will converge to a steady state, i.e. a constant value, when the self-cluster size grows beyond a critical value. However, the determination of this critical value would be computationally time consuming. Nonetheless, we can evaluate the steady state by considering a self-cluster with an infinite number of hydrogen atoms, i.e. the tungsten lattice is divided into two parts by a mono-layer of hydrogen atoms (see figure 2(e); this monolayer is referred to as H_∞ in the equation below), and the converged binding energy $E_b^{\text{H}_\infty}$ (i.e. $E_b^{\text{H}_n}$ with $n \rightarrow \infty$) is calculated by:

$$E_b^{\text{H}_\infty} = \frac{(N-1)E_{\text{tot}}^{\text{bulk}} + E_{\text{tot}}^{\text{H}_\infty} - NE_{\text{tot}}^{\text{H}_1}}{N}. \quad (8)$$

In this expression, $E_{\text{tot}}^{\text{bulk}}$ and $E_{\text{tot}}^{\text{H}_1}$ are quantities previously defined in equation (1), $E_{\text{tot}}^{\text{H}_\infty}$ is the total energy of the super-cell that contains a mono-layer of hydrogen (i.e. H_∞) that divides the tungsten lattice, and N is the number of hydrogen atoms within H_∞ in the super-cell. $E_b^{\text{H}_\infty}$ represents an average binding energy that can be considered as the steady-state binding energy of hydrogen for self-clusters that are beyond the critical size. According to our DFT calculations, this steady-state binding energy is found to be 0.38 eV when $n \rightarrow \infty$. The DFT-calculated data for different n are shown in figure 5. It is found that the data can be well fitted by a simple function, assuming the convergence scale to be $\alpha \exp(-n/\beta)$ (see figure 5(c)):

$$E_b^{\text{H}_n} = E_b^{\text{H}_\infty} - \alpha \exp(-n/\beta), \quad (9)$$

where the parameters α and β are fitted to be 0.45 eV and 12.04 , respectively.

3.3. Thermodynamic and kinetic analyses of hydrogen self-clustering

The preceding results demonstrate that hydrogen self-clustering is energetically possible in tungsten. Nevertheless, a comprehensive evaluation of the feasibility of hydrogen self-clustering under different temperatures and hydrogen concentrations necessitates further thermodynamic investigation, as elaborated in the following. During the formation of a H_n self-cluster, the Gibbs free energy change of the system, denoted as ΔG_n , is given as:

$$\Delta G_n = \Delta H - T\Delta S, \quad (10)$$

where ΔH and ΔS are the enthalpy and entropy changes, respectively, associated with the hydrogen aggregation reaction, i.e. $H_1 + H_1 + H_1 \cdots \rightarrow H_n$. According to our definition in equation (1), the enthalpy change can be evaluated as:

$$\Delta H = - \sum_{i=2}^n E_b^{\text{H}_i}. \quad (11)$$

⁵ See footnote 4.

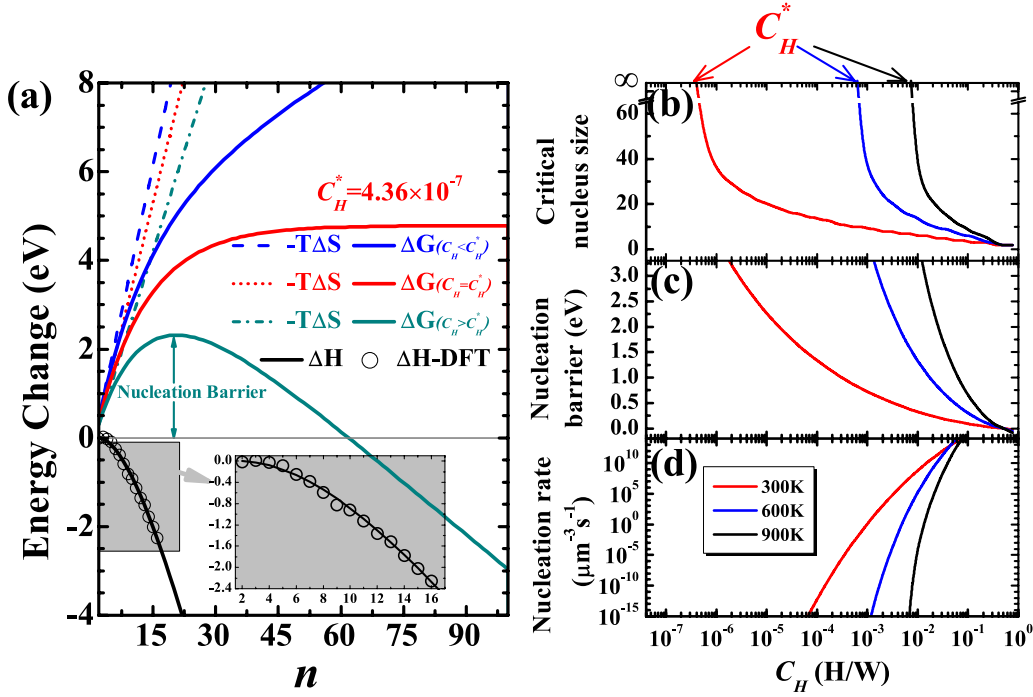


Figure 6. (a) Changes of free energy, enthalpy, and entropy term during self-clustering of H_n at 300 K with different hydrogen concentrations, calculated according to equations (9)–(12). Circles and lines represent DFT and analytical data, respectively. The red lines highlight the critical concentration at which the enthalpy and entropy cancel each other out. (b)–(d) Present the critical nucleus size, nucleation barriers, and nucleation rate of the hydrogen self-cluster as a function of hydrogen concentrations at 300, 600, and 900 K, respectively.

The entropy of a H_n cluster comprises of two parts, the translation entropy and configuration entropy [64]. However, the configuration entropy H_n is usually negligible, and thus the entropy change can be approximately given by (see⁶ for details):

$$\Delta S = (n-1)k_B \ln \frac{C_H}{1-C_H}, \quad (12)$$

where k_B is the Boltzmann constant and C_H is the bulk atomic concentration of hydrogen in tungsten (i.e. H/W ratio).

Based on equations (9)–(12), the Gibbs free energy change of the system as a function of the self-cluster size n at different C_H and $T = 300$ K is plotted in figure 6(a). We see that the enthalpy term ΔH decreases monotonically as n increases, with the rate of change in ΔH first accelerating and then gradually stabilizing at a constant rate. On the other hand, the term $-T\Delta S$ increases almost linearly with a rate depending on the hydrogen concentration. As illustrated in figure 6, the descending enthalpy as n increases provides a driving force for hydrogen self-clustering, which competes with the entropy effect that favors dissociation. Consequently, a critical hydrogen concentration C_H^* exists at which the enthalpy and entropy effects cancel each other out, and ΔG_n becomes a constant for large H_n self-clusters. According to equations (10)–(12), the critical concentration C_H^* is given by:

$$C_H^* = \frac{1}{\exp(E_b^H/k_B T) + 1}. \quad (13)$$

For $C_H < C_H^*$, ΔG_n increases monotonically as the self-cluster grows while, for $C_H > C_H^*$, ΔG_n first increases and then decreases as the self-cluster grows, indicating that it is thermodynamically possible for hydrogen cluster nucleation. The value of n where ΔG_n is maximized corresponds to the critical nucleus size, denoted as n_{nucl} , and the value of ΔG_n at n_{nucl} represents the associated nucleation barrier, marked by ΔG_{nucl} .

Figures 6(b) and (c) respectively present n_{nucl} and ΔG_{nucl} as functions of C_H at different temperatures. As shown in figure 6(b), the critical concentration C_H^* increases rapidly with the temperature, from 10^{-7} at 300 K and reaching 10^{-3} at 600 K. These concentrations are far greater than the hydrogen solubility in tungsten (10^{-23} at 300 K and 10^{-13} at 600 K under 1 bar of H_2 , extrapolated according to [65]). This suggests that the hydrogen self-clustering cannot occur under normal conditions (but can occur under high-flux hydrogen plasma charging, as we shall demonstrate in the following). The formation of hydrogen self-clusters becomes more difficult at high temperature, which is well expected because the entropy effect is stronger at higher temperatures. In addition, it is also clear from figure 6 that the critical nucleus size and nucleation barrier drops rapidly with the increase of hydrogen concentration. The hydrogen self-cluster can accordingly be formed more easily as C_H increases. We have further calculated the homogeneous nucleation rate of hydrogen self-clusters based on the classic nucleation theory [66]:

$$\Gamma_{\text{nucl}} = (\rho C_H)^2 D_H R_H Z \exp\left(\frac{-\Delta G_{\text{nucl}}}{k_B T}\right), \quad (14)$$

⁶ See footnote 4.

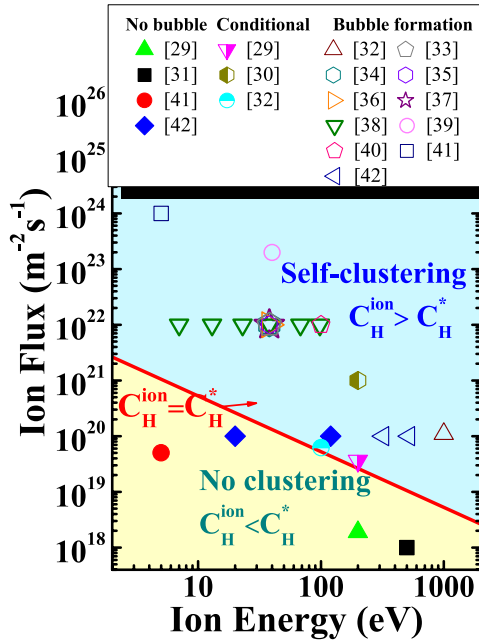


Figure 7. Hydrogen self-clustering ability under different hydrogen plasma loading fluxes and energies, calculated according to equations (13) and (15). The cyan-colored region maps the conditions that can result in self-clustering while the yellow-colored region corresponds to no-clustering conditions. The symbols denote experimental data at ~ 300 K from [29–42]. Hollow symbols represent bubble formation, filled ones represent no evident bubble formation, and half-filled ones represent that bubble formation also depends on variables other than ion energy and flux.

where ρ is the atomic density of tungsten, $D_H = 5.7 \times 10^{-8} \exp(-0.22 \text{ eV}/k_B T) \text{ m}^2 \text{ s}^{-1}$ is the diffusivity of hydrogen in tungsten [67], and $R_H = 0.223 \text{ nm}$ is the interaction range of between H–H at the most stable (4 nm) distance. Z denotes the Zeldovich factor, which is approximately a constant, $Z = 0.1$ [66]. The nucleation rates at different temperatures as functions of C_H are shown in figure 6(d), where we can see that the nucleation rate of the hydrogen self-cluster increases rapidly with C_H . Therefore, in higher hydrogen concentration environments, the hydrogen self-clustering is not only thermodynamically more favorable but also kinetically more feasible. The nucleation rate given by equation (14) agrees well with our benchmark object kinetic Monte Carlo simulations⁷, and also confirms some recent molecular dynamic studies [68, 69], where rapid nucleation of hydrogen self-clusters was observed under high hydrogen concentrations.

3.4. Possible mechanism of hydrogen bubble nucleation via self-clustering

From the preceding, we have shown that a necessary condition for H_n self-cluster formation is to have hydrogen concentration reach the critical concentration C_H^* . Though it is normally difficult for the hydrogen concentration to reach C_H^* due to the extremely low hydrogen solubility in tungsten, it can be possible when tungsten is exposed to low-energy, high-flux

hydrogen plasma (where the hydrogen concentration can reach up to 10^{-2} in some experiments [37, 39]). Generally, the maximum concentration of hydrogen under plasma implantation can be found at the implantation depth X . Considering that X is usually very small (a few nanometers) and hydrogen diffusion is fast (micrometers per second), the maximum hydrogen concentration C_H^{ion} , can be estimated using the stationary diffusion state of hydrogen into a semi-infinite tungsten bulk [70, 71]⁸:

$$C_H^{\text{ion}} = Xf/D_H, \quad (15)$$

where f is the incident flux of the hydrogen ion. Based upon our calculations using the TRIM code [72], the implantation depth X is approximately proportional to the incident ion energy, i.e. $X = E_H^{\text{ion}} \times 0.03 \text{ nm eV}^{-1}$.

In this way, the plasma flux and energy required for hydrogen self-clustering can be quantitatively predicted, i.e. $C_H^{\text{ion}} > C_H^*$. Figure 7 shows the results of our prediction at room temperature in comparison with available experimental results [29–42] (pre-annealed undamaged tungsten subjected to low-energy pure hydrogen plasma at around room temperature). The plot is divided into two regions by the condition of $C_H^{\text{ion}} = C_H^*$, respectively corresponding to where hydrogen self-clustering is predicted to occur (i.e. ‘self-clustering’ region) and not occur (‘no clustering’ region). As seen in figure 7, the loading experimental plasma conditions that cause significant bubble formation (indicated by hollow symbols) fall well within the self-clustering region, while those without evident bubble observation (indicated by solid symbols) fall within the no-clustering region. This excellent agreement between experimental observations and theoretical prediction suggests that hydrogen self-clustering is closely related to hydrogen bubble formation.

The connection between hydrogen self-clustering and hydrogen bubble formation was also reflected by a few earlier experiments [25, 73, 74], where cleavage cracks in iron were induced by electrochemical hydrogen charging even when no external strain was applied. The cleavage cracks were observed to initiate and propagate along the $\{001\}\langle 110 \rangle$ directions, accompanied by clear dislocation emission. In light of these experiments and our results, below we propose a possible mechanism for the hydrogen bubble nucleation by hydrogen self-clustering. When excessive interstitial hydrogen atoms exist in the tungsten lattice, they gather together to form thin single or multi-layered platelets along the $\{001\}$ lattice planes to reduce the strain energy of the system. Once the platelet hydrogen self-cluster forms, it induces noticeable lattice bending and weakens metallic bonds around the platelet (see figure 8(a)). As suggested by Fujita [51], dislocations can be created at the platelet edge so as to further release the elastic energy. The dislocation emission can make room for interstitial hydrogen atoms in the platelet self-cluster to convert to hydrogen adatoms (see figure 8(b)), which can lower the energy⁹. This would further increase the lattice bending around the platelets and induce more severe loosening of the

⁸ See footnote 4.

⁹ See footnote 4.

⁷ See footnote 4.

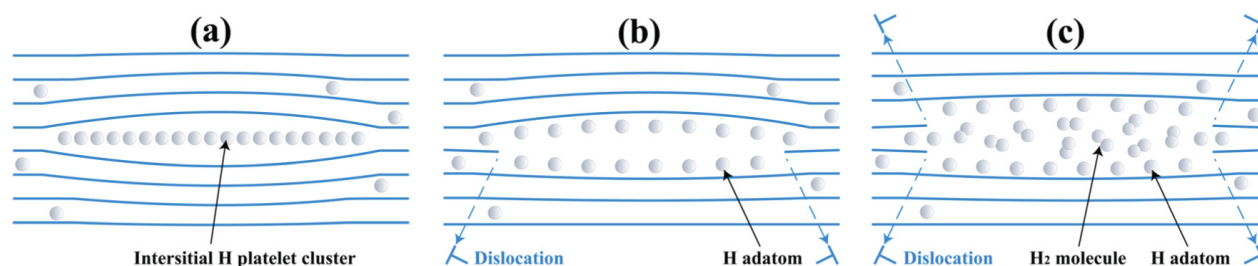


Figure 8. Schematic representation of the process of platelet aggregation of hydrogen atoms and spontaneous bubble formation in a perfect tungsten lattice. The hydrogen atoms are represented by small white balls.

lattice cohesion, eventually causing a slight opening of the lattice. As this process continues, adatoms would accumulate and get desorbed to produce H_2 gas in the opening. The internal gas pressure would be conducive to the further growth of the opening and ultimately give rise to spontaneous crack (hydrogen bubble) formation (see figure 8(c)).

The dislocation emission mechanism just proposed allows hydrogen self-clusters to convert to hydrogen bubbles in a defect-free tungsten. This is in accordance with many recent experimental observations showing that hydrogen bubbles can form even in fully recrystallized tungsten samples [20, 33, 34, 43], and large density of dislocations along with hydrogen bubble formation were found in tungsten after high-flux plasma loading [19, 50]. Furthermore, the emitted dislocations can glide and transport tungsten atoms toward the surface to subsequently cause surface blistering. Considering the preferential growth of platelet-like hydrogen self-clusters and available slip systems in bcc tungsten, we may also expect a certain dependence of surface blister formation on the grain orientation¹⁰, a phenomenon observed in several previous experiments [34, 43, 75]. Another point worth noting about the mechanism is that as dislocations (and other associated defects) start to form, they will also induce stress fields and provide heterogeneous nucleation sites which could further influence hydrogen self-clustering and subsequently hydrogen bubble formation. These aspects require detailed knowledge regarding the interplay between lattice defects and hydrogen self-clustering, which certainly necessitates further dedicated studies.

4. Conclusions

In summary, this work studied the self-clustering of hydrogen atoms within the tungsten lattice using first-principles calculations. Possible hydrogen self-cluster structures have been examined. It was found that hydrogen atoms would form 2D platelet-like structures, preferentially along $\{100\}$ planes. The hydrogen self-cluster was shown to be energetically more favorable as the cluster size increases, suggesting the increasing ability of a hydrogen self-cluster to capture additional interstitial hydrogen. These hydrogen self-clustering behaviours can be well understood by the competition between long-ranged elastic attraction and local electronic repulsion, which were both isolated and evaluated quantitatively. Further

thermodynamic analysis showed that there exists a critical hydrogen concentration, above which hydrogen self-clusters are thermodynamically stable and kinetically feasible, and below which all hydrogen self-clusters become unfavorable. Based on this critical hydrogen concentration, the plasma-loading conditions required for hydrogen self-cluster formation are predicted. Our theoretical predictions show excellent agreement with the experimental results of hydrogen bubble formation in tungsten exposed to low-energy hydrogen irradiation, suggesting close connections between hydrogen self-clustering and hydrogen bubble formation. Based on our findings, we propose that the lattice bending induced by platelet-like hydrogen self-clusters may trigger dislocation emissions to release the system energy, which provides rooms for H_2 gas precipitation and finally leads to spontaneous bubble formation. The present study provides mechanistic insights and quantitative models towards the understanding of plasma-induced hydrogen bubble formation in plasma-facing metals.

Acknowledgment

This work is supported by the National Key Research and Development Program of China (Grant No.: 2017YFA0402800), the National Natural Science Foundation of China (Nos.: 11505229, 11735015, 51771185, 11505214), and by the Natural Sciences and Engineering Research Council of Canada (NSERC) Discovery grant (Grant No. RGPIN 418469-2012). We also thank the Center for Computation Science, Hefei Institutes of Physical Sciences, and the Supercomputer Consortium Laval UQAM McGill and Eastern Quebec. J. Hou acknowledges financial support from the China Scholarship Council (CSC).

ORCID iDs

C. S. Liu  <https://orcid.org/0000-0003-1009-1367>

References

- [1] Xie D.G. et al 2015 *Nat. Mater.* **14** 899–903
- [2] Tiegel M.C. et al 2016 *Acta Mater.* **115** 24–34
- [3] Rozenak P. et al 2007 *Int. J. Hydrog. Energy* **32** 2816–23
- [4] Condon J.B. et al 1993 *J. Nucl. Mater.* **207** 1–24
- [5] Becquart C.S. et al 2006 *Phys. Rev. Lett.* **97** 196402

¹⁰ See footnote 4.

- [6] Kong X.S. *et al* 2016 *Nucl. Fusion* **56** 106002
- [7] Kong X.S. *et al* 2016 *Nucl. Fusion* **56** 026004
- [8] Henriksson K.O.E. *et al* 2005 *Appl. Phys. Lett.* **87** 163113
- [9] Becquart C.S. *et al* 2009 *J. Nucl. Mater.* **386–8** 109–11
- [10] Liu Y.L. *et al* 2009 *J. Nucl. Mater.* **390–1** 1032–4
- [11] You Y.W. *et al* 2014 *Nucl. Fusion* **54** 103007
- [12] Monasterio P.R. *et al* 2009 *Phys. Rev. Lett.* **103** 085501
- [13] Ouyang C. *et al* 2011 *Phys. Rev. B* **83** 045111
- [14] Von Pezold J. *et al* 2011 *Acta Mater.* **59** 2969–80
- [15] Zhou X. *et al* 2016 *Phys. Rev. Lett.* **116** 075502
- [16] Valles G. *et al* 2017 *Acta Mater.* **122** 277–86
- [17] Zhou H.B. *et al* 2010 *Nucl. Fusion* **50** 025016
- [18] Xiao W. *et al* 2012 *J. Nucl. Mater.* **430** 132–6
- [19] Terentyev D. *et al* 2014 *Nucl. Fusion* **54** 042004
- [20] Terentyev D. *et al* 2015 *J. Appl. Phys.* **117** 083302
- [21] De Backer A. *et al* 2018 *Nucl. Fusion* **58** 016006
- [22] Kong X.S. *et al* 2013 *J. Nucl. Mater.* **433** 357–63
- [23] Geng W.T. *et al* 2017 *Scr. Mater.* **134** 105–9
- [24] Sun L. *et al* 2016 *Scr. Mater.* **122** 14–7
- [25] Tetelman A.S. *et al* 1963 *Acta Metall.* **11** 415–26
- [26] Ren X.C. *et al* 2008 *Metall. Mater. Trans. A* **39** 87–97
- [27] Escobar D.P. *et al* 2011 *Corros. Sci.* **53** 3166–76
- [28] Poon M. *et al* 2005 *J. Nucl. Mater.* **337–9** 629–33
- [29] Alimov V.K. *et al* 2005 *J. Nucl. Mater.* **337–9** 619–23
- [30] Alimov V.K. *et al* 2008 *J. Nucl. Mater.* **375** 192–201
- [31] Poon M. *et al* 2002 *J. Nucl. Mater.* **307–11** 723–8
- [32] Wang W. *et al* 2001 *J. Nucl. Mater.* **299** 124–31
- [33] Shu W.M. *et al* 2007 *Nucl. Fusion* **47** 201–9
- [34] Shu W.M. *et al* 2007 *Phys. Scr.* **T128** 96–9
- [35] Shu W.M. *et al* 2008 *Fusion Eng. Des.* **83** 1044–8
- [36] Alimov V.K. *et al* 2009 *Phys. Scr.* **T138** 014048
- [37] Alimov V.K. *et al* 2012 *J. Nucl. Mater.* **420** 519–24
- [38] Luo G.N. *et al* 2005 *J. Nucl. Mater.* **347** 111–7
- [39] Zibrov M. *et al* 2017 *Nucl. Fusion* **57** 046004
- [40] Tokunaga K. *et al* 2005 *J. Nucl. Mater.* **337–9** 887–91
- [41] Zayachuk Y. *et al* 2015 *J. Nucl. Mater.* **464** 69–72
- [42] Ni W. *et al* 2015 *J. Nucl. Mater.* **464** 216–20
- [43] Zayachuk Y. *et al* 2016 *Nucl. Fusion* **56** 086007
- [44] Buzi L. *et al* 2014 *J. Nucl. Mater.* **455** 316–9
- [45] Buzi L. *et al* 2015 *J. Nucl. Mater.* **463** 320–4
- [46] Jia Y.Z. *et al* 2017 *Nucl. Fusion* **57** 034003
- [47] Fukai Y. *et al* 2003 *J. Alloys Compd.* **356–7** 263–9
- [48] Sugimoto H. *et al* 2014 *Acta Mater.* **67** 418–29
- [49] Sugimoto H. *et al* 2017 *Scr. Mater.* **134** 20–3
- [50] Terentyeva D. *et al* 2017 *Fusion Eng. Des.* **124** 405–9
- [51] Fujita F.E. 1976 *Trans. JIM* **17** 232–8
- [52] Kamachi K. *et al* 1972 *Proc. Int. Conf. Mech. Behav. Mater.* **3** 274
- [53] Kresse G. *et al* 1993 *Phys. Rev. B* **47** 558–61
- [54] Kresse G. *et al* 1996 *Phys. Rev. B* **54** 11169–86
- [55] Blochl P.E. 1994 *Phys. Rev. B* **50** 17953
- [56] Perdew J.P. *et al* 1992 *Phys. Rev. B* **46** 6671
- [57] Perdew J.P. *et al* 1993 *Phys. Rev. B* **48** 4978
- [58] Murali D. *et al* 2015 *Phys. Rev. B* **92** 064103
- [59] Switendick A.C. 1979 *Z. Phys. Chem.* **117** 89
- [60] Fukai Y. 2005 *The Metal-Hydrogen System-Basic Bulk Properties* 2nd edn (Berlin: Springer)
- [61] Kittel C. 1986 *Introduction to Solid State Physics* 6th edn (New York: Wiley)
- [62] Henkelman G. *et al* 2006 *Comput. Mater. Sci.* **36** 354–60
- [63] Sanville E. *et al* 2007 *J. Comput. Chem.* **28** 899
- [64] Kapur S.S. *et al* 2005 *Phys. Rev. B* **72** 014119
- [65] Frauenfelder R.J. 1969 *Vac. Sci. Technol.* **6** 388
- [66] Sear R.P. 2007 *J. Phys.: Condens. Matter* **19** 033101
- [67] Kong X.S. *et al* 2015 *Acta Mater.* **84** 426–35
- [68] Chen Z. *et al* 2016 *J. Nucl. Mater.* **481** 190–200
- [69] Cusentino M.A. *et al* 2015 *J. Nucl. Mater.* **463** 347–50
- [70] Doyle B.L. *et al* 1982 *J. Nucl. Mater.* **111–2** 628
- [71] Kolasinski R.D. *et al* 2015 *J. Appl. Phys.* **118** 073301
- [72] Ziegler J.F. *et al* 1985 *The Stopping and Range of Ions in Solids* (New York: Pergamon)
- [73] Marrow T.J. *et al* 1996 *Acta Mater.* **44** 3125–40
- [74] Chen X. *et al* 1990 *Eng. Fract. Mech.* **35** 997–1017
- [75] Jia Y.Z. *et al* 2016 *J. Nucl. Mater.* **477** 165–71